Detailed characterization of the early x-ray emission of a plasma produced by point-like laser irradiation of solid Al targets

L. Labate,[a),b)] C. A. Cecchetti,[c)] M. Galimberti,[a)] A. Giulietti,[a)]
D. Giulietti,[d)] and L. A. Gizzi[a)]
Intense Laser Irradiation Laboratory-Istituto per i Processi Chimico-Fisici (IPCF)
[Consiglio Nazionale delle Ricerche (CNR)], Pisa, 56124, Italy[e)]

(Received 23 February 2005; accepted 8 June 2005; published online 12 August 2005)

A study of the dynamics of the x-ray emission from a point-like Al plasma produced by tight-focusing laser irradiation of a thick target is reported. Two-dimensional maps of the x-ray emission calculated at selected wavelengths show that, due to the rapid expansion cooling, x-ray emission mostly originates from a thin spatial layer. These properties enabled the results of the simulations to be compared with time-resolved x-ray spectra obtained under well-controlled experimental conditions. The outcome of this comparison is discussed in details, in view of the results reported in a recently published Letter [L. A. Gizzi, C. A. Cecchetti, M. Galimberti, A. Giulietti, D. Giulietti, L. Labate, S. Laville, and B. Tomassini, Phys. Plasmas **10**, 4601 (2003)]. Moreover, the x-ray-reabsorption issues and the role of the Doppler decoupling mechanism in the presence of the strong velocity gradient typical of our experimental condition are discussed, also in view of a possible dedicated experiment. © *2005 American Institute of Physics*.
[DOI: 10.1063/1.1987618]

I. INTRODUCTION

Laser-produced plasmas are characterized by several physical parameters, including ionization degree, electron density, and electron temperature. The values of these parameters depend upon the relative roles played by the different mechanisms of absorption of the laser energy. Due to the high temperatures reached at even moderate laser intensities, resulting in a strong x-ray emission, these plasmas are the subject of investigations in many fields of applied and fundamental research, from laser-plasma sources for lithography,[1] microscopy,[2] and coronary angiography (see Refs. 3 and 4 and references therein) to x-ray lasers,[5] and from inertial confinement fusion[6,7] (ICF) to laboratory astrophysics.[8] For the understanding of the thermodynamic and radiative properties of such plasmas in the laboratory it is essential that accurate, independent measurements of the density and temperature are performed. This can be done, for example, by using optical probing interferometry[9–12] or Thomson scattering diagnostics.[13–15] However, in the case of plasmas produced by solid targets, these diagnostics are limited to the outer regions of the plasma, far from the critical region. Recently, picosecond interferometry of laser-produced plasmas using a soft-x-ray laser has been performed,[16] which demonstrates the possibility of probing the plasma regions at higher electron density.

On the other hand, it is well known that the spectrum of the x-ray radiation generated by a laser-produced plasma contains a wealth of information about the inner plasma condition. For this reason, x-ray spectroscopy is regarded as a powerful tool to investigate even the denser regions of high-temperature plasmas (see Ref. 17 and references therein). Unfortunately, a detailed understanding and modeling of the x-ray line or continuum emission from laser plasmas is a complex task even for relatively simple spectra like those originating from one- or two-electron ions (*K*-shell spectra). In fact, from a theoretical viewpoint, this would require the knowledge, at any time and position inside the plasma, of the ionization equilibrium. In other words, since rapidly changing hydrodynamic conditions, both in space and time, are found to exist in laser plasmas, this means that the equations governing the hydrodynamic motion as well as a suitable system of rate equations, where a spatial dependence is included, must be solved simultaneously. Also, apart from selected regions, a nonlocal thermodynamic equilibrium (NLTE) is to be considered. Furthermore, the radiative-transfer problem, involving the absorption and emission of radiation along a propagation path inside the plasma, must in principle be taken into account.[18] In fact, the latter process can lead to a significant modification in the intensities and profiles of the lines in the emission spectrum and must therefore be included when studying the x-ray-emission properties.

A convenient and commonly used approach to the problem of modeling x-ray spectra from laser plasmas is to decouple the hydrodynamics from the atomic physics. In other words, a simplified atomic model is supplied, providing a reliable estimate of ionization for calculating the plasma energy balance, for the hydrodynamic simulations.[19,20] The hydrodynamic data generated in this way can then be postprocessed to generate synthetic x-ray emission spectra.[21] In this

[a)]Also at INFN, Sezione di Pisa, Italy.
[b)]Electronic mail: luca.labate@ipcf.cnr.it
[c)]Presently at Department of Pure and Applied Physics, The Queen's University of Belfast, Belfast, United Kingdom.
[d)]Also at Dipartimento di Fisica, Università di Pisa, and INFN, Sezione di Pisa, Italy.
[e)]URL: http://ilil.ipcf.cnr.it

second step, the radiative-transfer problem is dealt with using a multicell approach.[22]

From an experimental viewpoint, test plasmas are usually produced under controlled laser irradiation conditions to minimize uncertainties on the knowledge of plasma parameters. This is of a crucial importance, for example, when test plasmas are used for the benchmarking of atomic-physics codes.[23,24] Furthermore, a controlled plasma hydrodynamic expansion is of a major concern in order to account for x-ray reabsorption issues in the simulations.[22]

Test plasmas are typically produced using picosecond or nanosecond (ns) laser pulses focused on the surface of a solid thick target[25] or using exploding foils.[26] Often, a predominantly one-dimensional (1D) (planar) expansion is tentatively allowed for by suitable target configurations based on microdot targets.[27] However, regardless of the test plasma configuration used, recent experiments[13,28] consistently suggest that, even in plasmas dominated by a planar expansion, two- or three-dimensional hydrodynamic effects at the plasma boundaries may play a significant role when attempting to model the x-ray-emission properties.

The role of hydrodynamics becomes critical in the transient regime of plasma formation, when the x-ray emission arises from plasma regions characterized by rapid changes and strong spatial gradients of hydrodynamic quantities. In these circumstances the modeling of x-ray spectra requires fully time-dependent atomic physics and multidimensional hydrodynamics with radiative-transfer calculations. In fact, as it is well known, an important simplification in the matrix problem defining the plasma ionization equilibrium can be made when changes in the hydrodynamic parameters of the plasma occur on a time scale that is much greater than the time scale for the atomic processes. In such a case the plasma is considered to be in a steady state for what concerns its ionization equilibrium. In other words, a solution of the rate equations with $dN_Z^i/dt=0$, where N_Z^i is the population of the ith level of the ion charge state Z, can be independently looked for at any time, using the values for the electron density and temperature provided by the hydrodynamic simulations at that time. For an Al plasma in conditions usually obtained by focusing ns laser pulses onto solid targets, simple estimates[29,30] indicate that the atomic relaxation times for reaching the H-like charge state starting from the He-like charge state are comparable with the rise time of a ns laser pulse, like those typically used in ICF-related studies. Thus, the change in the hydrodynamic variables are expected to come into play when modeling the early-stage plasma formation, possibly leading to different predictions in the x-ray spectra when time-dependent (TD) or steady-state (SS) solutions of the ionization equilibrium rate equations are considered.

As pointed out above, the study of the ionization and emission dynamics is usually performed by producing a plasma whose expansion geometry is predominantly planar. This requires the irradiation of a large target surface. As a consequence, large spot sizes are required, so that this kind of study is usually performed at large-scale laser facilities.[27,28] A different approach consists of using a "point-like" laser irradiation, i.e., using a laser spot size smaller than the density and temperature scale lengths expected at the peak of the pulse. The plasma produced in this way is characterized by rapidly changing hydrodynamic conditions. In these circumstances the plasma expansion can be profitably modeled, using two-dimensional (2D) hydrodynamic codes, by exploiting the cylindrical symmetry of the interaction geometry. Motivated by the above considerations, we performed an experiment aimed at investigating the early-stage plasma formation, i.e., the plasma evolution at times comparable to the relaxation times of the ionization of the target starting from the cold material. Our measurements clearly show that, in spite of the relatively long (ns) laser-pulse duration, a condition is obtained during the ionization stage in which changes in hydrodynamic parameters of the x-ray emitting plasma occur on a faster time scale than the typical time scale of ionization, as preliminarly reported in a recently published Letter.[29] In this paper, a complete description of the hydrodynamics and x-ray emission properties of an Al plasma produced by point-like laser irradiation as the one concerned in Ref. 29 is given, in particular, during the rise time of the laser pulse, including the results of time-resolved x-ray spectroscopy. In detail, the temporal and spatial features of the early x-ray emission from the plasma are investigated, based mainly on hydrodynamic and kinetic simulations. This paper focuses on the study of the x-ray reabsorption effects in our experimental conditions, leading to interesting conclusions on the plasma opacity and precise suggestions for future studies.

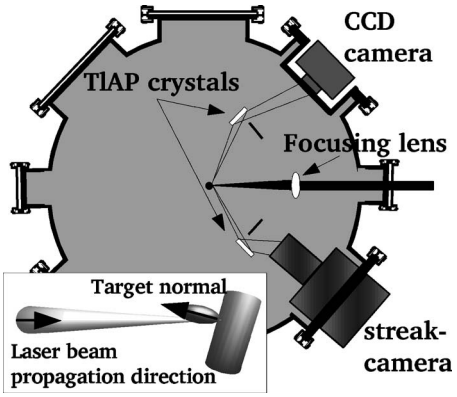

FIG. 1. Experimental setup for the time-resolved study of the plasma x-ray emission. The two main diagnostics, namely, the time-integrating and the time-resolving Bragg spectrometers, are clearly visible inside the interaction chamber. In the inset the geometrical arrangement of the Al cylindrical target is shown: the main axis of the target is tilted by 20° with respect to the vertical direction in order to enable a simultaneous detection by the two symmetric x-ray spectrometers and, at the same time, to avoid harmful back reflections of the laser beam.

II. EXPERIMENTAL SETUP AND METHODS

The experiment was carried out at the Intense Laser Irradiation Laboratory (ILIL) of the IPCF-CNR in Pisa (Italy). A layout of the experimental setup inside the interaction chamber is shown in Fig. 1.

A Nd:yttrium lithium flouride (YLF) laser pulse, with a duration of 3 ns [full width at half maximum (FWHM)] and a total energy of about 3 J, was focused on a cylindrical Al

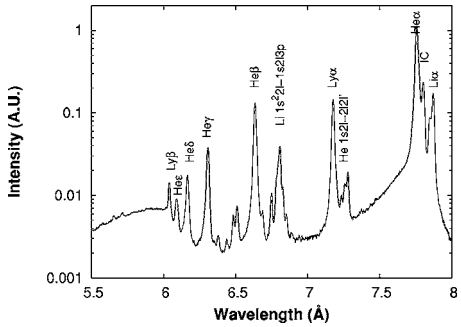

FIG. 2. X-ray-emission spectrum of the produced plasma, obtained using the time-integrating spectrometer.

target by means of an $f/4$ lens. Due to its good spatial quality, the beam was focused in a spot size of about 6 μm. This beam diameter, which results in a maximum nominal intensity on the target of the order of 10^{15} W/cm^2, is significantly smaller than those typically used at large-scale facilities for this class of experiments, in which much more energy is delivered on the target at nearly the same intensity.[27,28] As it will be shown later, this has important consequences on the plasma hydrodynamics. A crucial issue in the investigation of the x-ray-emission dynamics shown here is the feature of our laser system that enables it to generate a single longitudinal-mode pulse, thus providing a "clean," Gaussian-shaped temporal profile, free from the "spiky" behavior typical of the laser pulses characterized by a multimode oscillation. These circumstances enabled us to produce a highly reproducible plasma,[31] with a smooth temporal behavior.

The two x-ray spectrometers, a time-integrating and a time-resolving one, were both equipped with a flat TlAP crystal mounted in a first-order Bragg configuration as a dispersive element. Both spectrometers were set to view the plasma at an angle of about 65° from the normal to the target surface. The time-integrating spectrometer was equipped with a back-illuminated, high-dynamic range, Peltier-cooled charge-coupled device (CCD) camera. Figure 2 shows a typical spectrum obtained with such a spectrometer in the spectral range from 5.5 to 8.0 Å, enclosing the main lines from the ion charge states Al XI (Li-like), Al XII (He-like), and Al XIII (H-like). The spectral resolution of this spectrum, depending on the crystal rocking angle, the plasma size, and the detector-sensitive element size,[32] was estimated to be $\delta\lambda/\lambda \simeq 7.1\times 10^{-3}$.

The detector of the time-resolving spectrometer was a streak camera, fitted with a 10-μm-thick, CsI-coated photocathode and a 1-mm-wide entrance slit. An example of a typical time-resolved spectrum after removal of a pincushion-like aberration typical of electron as well as intensifier screen imaging optics has been reported in Ref. 29. In particular, the resonance series of the He-like ions and the main resonance line of the H-like ions including the corresponding satellites have been studied with a time resolution of about 20 ps. The spectral resolution was mainly limited by the energy spreading of the photoelectrons in the photocathode and was about $\delta\lambda/\lambda \simeq 1.4\times 10^{-2}$.

The system consisting of the streak camera, the intensifying device, and the corresponding optical imaging system was calibrated using an original experimental method that enabled us to minimize the uncertainty in the relative intensity calibration of the time-resolved spectra. As shown in the inset of Fig. 1, both spectrometers are set to view the plasma along lines of sight that are symmetric with respect to the local target normal. In these circumstances the x-ray radiation incident on the two spectrometers is expected to exhibit the same spectral properties. This enabled an accurate cross calibration of the intensity of the streak-camera detector using the CCD camera as a reference.[33] In fact, due to the intrinsic high linearity of the CCD detector, spectra obtained with this system can be considered our reference spectra for relative intensity calibration. Spectra obtained simultaneously by the streak-camera system running in dc, time-integrating mode are then compared with analogous CCD ones. In this condition the relative spectrum of the radiation impinging on the streak-camera photocathode, $I^0_{\mathrm{tr}}(\lambda)$, can be expressed as a function of the spectrum of the radiation provided by the time-integrating spectrometer $I_{\mathrm{ti}}(\lambda)$ as

$$I^0_{\mathrm{tr}}(\lambda) = \frac{T_{\mathrm{tr}}(\lambda) I_{\mathrm{tr}}(\lambda)}{T_{\mathrm{ti}}(\lambda) S_{\mathrm{CCD}}(\lambda)}, \tag{1}$$

where $T_{\mathrm{tr}}(\lambda)$ and $T_{\mathrm{ti}}(\lambda)$ account for the transmission of the filters used for the time-resolving and the time-integrating spectrometer, respectively, and $S_{\mathrm{CCD}}(\lambda)$ is the CCD spectral response. A functional form of the formula giving the intensity response of the time-resolving spectrometer can thus be found by fitting a set of data $\{I^0_{\mathrm{tr}}(\lambda_i), I_{\mathrm{tr}}(\lambda_i)\}$, each corresponding to a given spectral line λ_i, using a suitable function $I_{\mathrm{tr}}(I^0_{\mathrm{tr}}) = f(I^0_{\mathrm{tr}})$. Here $I_{\mathrm{tr}}(\lambda)$ is the signal provided by the system and $I^0_{\mathrm{tr}}(\lambda)$ is given by (1). The data points can be taken as the intensities of different spectral lines λ_i. In our case the calibration curves were obtained by fitting these data points using functions of the form $f(x) = ax^b$. The calibration curves obtained in this way were then used to correct the time-resolved spectra.

In general, plasma conditions are inferred from x-ray emission spectra by comparing line intensity ratios or line-to-continuum ratios with predictions of kinetic simulations. In particular, informations on the electron temperature can be obtained by the intensity ratio between emission lines originating from different ionization stages. From a theoretical viewpoint, great care must be taken when considering the reabsorption effect. This is particularly true in the case of resonance lines from the first excited level to the ground state (see, for example, Ref. 17). In our case, for the analysis which is described below, we used the Heβ line for the He-like Al stage, while, concerning the H-like stage, signal-to-noise considerations led us to use the Lyα resonance line. As we will discuss below, great care has been taken to evaluate opacity effects. The time behavior of the Lyα-to-Heβ ratio was then considered, in particular, during the early-stage plasma formation, i.e., during the rising edge of the laser pulse, with a time resolution of about 20 ps.

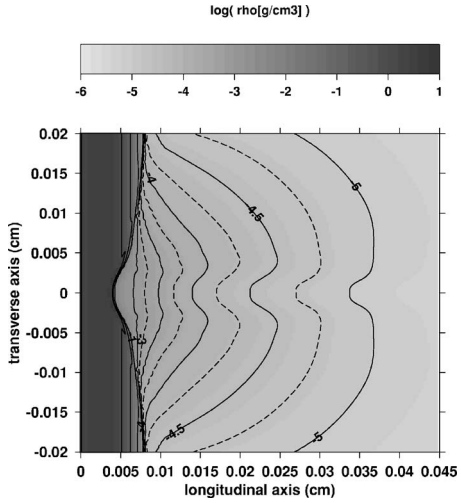

FIG. 3. Mass density map of the Al plasma produced by a tightly focused 3-ns laser pulse at its intensity peak as calculated by the 2D hydrodynamic code POLLUX. The laser intensity used for the simulation is $I_{max} = 10^{14}$ W/cm^2 and the Gaussian beam waist is 6 μm. The initial position of the target surface is located at 0.005 cm and the laser beam impinges from the right.

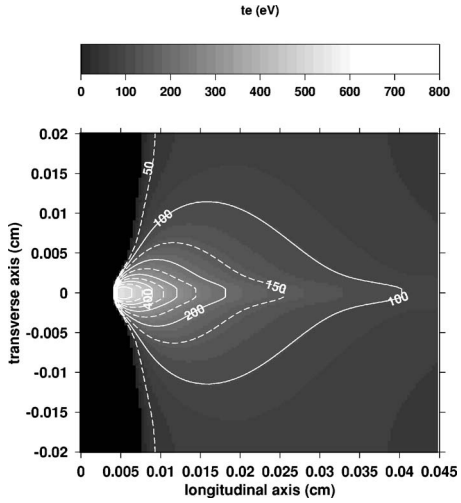

FIG. 4. Electron temperature map of the Al plasma in the same conditions as of Fig. 3.

III. RESULTS AND DISCUSSION

A. Plasma hydrodynamic modeling

The hydrodynamic behavior of the plasma produced in our experiment has been modeled by using the 2D code POLLUX.[34,35] The simulation box was 450 μm in the longitudinal (i.e., plasma expansion) direction and 200 μm in the transverse direction. The focal spot of the laser had a Gaussian profile with 6 μm FWHM and the pulse time profile was set to be Gaussian with a 3 ns FWHM pulse width. The intensity on the target was set to be 1×10^{14} W/cm^2. We observe that this value is significantly lower than the nominal experimental one. In fact, the hydrocode does not account for mechanisms, such as Brillouin backscattering and other instabilities, that lead to a reduction of the effective laser intensity on target. In our case, the appropriate value of the laser intensity to be used in the simulation was found adopting a *post facto* approach. In particular, since our study was mainly devoted to a comparison of the early x-ray emission with both SS and TD simulations, we compared modeling predictions and experimental results at late times, i.e., for times where no transient effects are expected, so that both SS and TD x-ray-emission simulations are expected to give identical results which can be safely compared with the observed x-ray line intensities. This comparison is independent of the conclusions of the investigation at early times and can therefore be used to validate the modeling procedure. Additionally, we used independent time-integrated x-ray spectra to compare time-averaged temperatures with those predicted by the modeling. In other words, we were able to "tune" the value of the laser intensity to be used in the simulation by ensuring that independent measured quantities were in agreement with calculated ones.

Figures 3 and 4 show, respectively, the mass density and the electron temperature maps provided by the simulation at the peak of the laser pulse. The simulated region was limited to positive values of the transverse coordinate. The maps, extending for negative values, too, were then obtained, for a better visualization, by replicating the data for positive values. This is possible because of the cylindrical symmetry across the plasma expansion axis assumed by the code. Strong 2D features of the plasma expansion are clearly visible in the figures and, according to the simulations, this behavior holds at all times during the laser pulse. In general, 2D effects in the plasma hydrodynamic expansion can be seen to play a minor role up to distances from the original target surface comparable to the size of the laser focal spot.[36] According to the figures, the small spot size (due to the tight focusing) allowed us to produce a plasma whose expansion was predominantly spherical. Under such conditions, the plasma exhibits high spatial gradients of its hydrodynamic parameters and a rapid cooling of the coronal region. These circumstances give rise to highly inhomogeneous longitudinal profiles of the main plasma parameters, such as electron density and temperature and expansion velocity. Later on, these conditions will be seen to have general, important consequences on the x-ray emission and reabsorption properties of the plasma.

B. Spatial and temporal issues in the modeling of X-ray spectra

In order to investigate the x-ray-emission dynamics of the plasma during the startup phase, both a steady-state and a time-dependent modeling of the Lyα-to-Heβ intensity ratio as a function of time have been carried out. This was done using the kinetic code FLY,[37] which solves the rate equations governing plasma ionization in a collisional-radiative equilibrium. The detailed structure of the levels with principal quantum numbers from 1 to 10 is considered by the code for the H-, He- and Li-like charge states (for the latter two, simplified hydrogenic formulas are used for $n \geq 6$), and only the ground state for lower charge states is included. The rate equations are solved on a single cell, that is, no spatial dependence is considered. Radiation trapping is included through the so-called escape factors.[22,37,38]

In order to model the Lyα-to-Heβ intensity ratio as a function of time, the histories of the electron density $n_e(t)$ and temperature $T_e(t)$ are needed. If we consider the largely inhomogeneous plots of Figs. 3 and 4, a question arises at this point concerning the position inside the plasma at which these two quantities should be taken. In principle, since the experimental data are space integrated over the entire plasma, a rigorous comparison would require a calculation of the intensity of each line over the entire plasma profile. On the other hand, simple physical arguments can be adopted to ease the procedure.

In previous works carried out at the same irradiation conditions,[31,39] where a spatially resolved study of the plasma was performed, most of the x-ray emission was found to originate from regions where the electron density was in the range between 5×10^{20} and 1×10^{21} cm^{-3}, that is, the regions where the electron density is slightly smaller than the critical density for a Nd laser ($n_{\mathrm{cr},1\ \mu\mathrm{m}}\simeq10^{21}$ cm^{-3}). This was also inferred from the simulations that show that most of the laser energy is absorbed near the critical density. Following this suggestion, a constant density could be considered and the corresponding temperature history could be gained by the hydrodynamic simulations. As we will see below in this section, while this approach is acceptable for a study of the plasma x-ray emission at times "not so far" from the peak of the laser pulse, it is not valid when dealing with plasma ionization dynamics during the early-stage plasma formation. In our case we used a less-simplified approach that accounts for the 2D spatial and temporal dynamics of the emission.

In detail, the 2D density and temperature maps provided by the hydrodynamic simulation were postprocessed by the code FLY so as to get, at each time, a map of the emissivity for both the Lyα and Heβ lines. This task was undertaken on each cell of the mesh used for the hydrodynamic simulation. Figures 5 and 6 show the 2D maps, at different times during the laser pulse, for the emission of the Lyα and the Heβ lines. These maps are normalized to the maximum local value of the emission of the two lines reached during the whole pulse duration. Figure 7 shows instead the history of these maxima for the two lines. Although the maximum of the local emission occurs for both lines at the peak of the laser pulse, a different behavior is found for the time history of the two lines. In general, Figs. 5 and 6 show that the instantaneous emission for both the Lyα and Heβ lines mostly originates from a plasma region, having a transverse size similar to that of the laser focal spot, located near the target surface, where, according to Fig. 3, a nearly planar expansion takes place.

These figures also show that the longitudinal profiles of the emission at each time exhibit a narrow peak, sitting on a long tail due to the plume of the plasma. The location of the peak moves inward by approximately 10 μm during the entire laser pulse. According to these results, at each time frame, characteristic values of the electron temperatures and densities exist corresponding to the position of the maximum emissivity at each time. This observation allowed us to assume these values as the reference values for the modeling of the x-ray spectrum as discussed above. In particular, the Heβ line was chosen for this purpose. However, similar results as

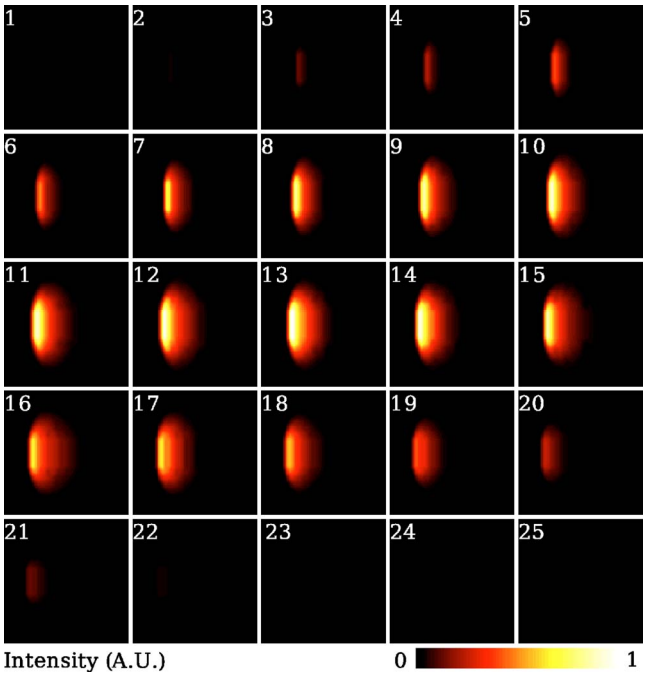

FIG. 5. (Color online). Calculated 2D maps of the x-ray emission at the Lyα emission wavelength at different times with respect to the peak of the laser pulse. Each frame corresponds to a different time with respect to the peak of the laser pulse, located at frame No. 13. The time interval between successive frames is 100 ps, so that frame No. 1 (No. 25) corresponds to 1.2 ns before (after) the pulse peak. The horizontal scale goes from −25 to 75 μm, the original target surface being located at 0 μm and the laser beam impinging from the right. The vertical scale ranges from −25 to 25 μm. The intensity is normalized to the maximum of the Lyα and the Heβ emissivity during the whole pulse duration.

those described below, in particular, at early times, can be obtained by taking into account the hydrodynamic values of density and temperature calculated by the Lyα emission maps. Figures 8 and 9 show the histories of the electron temperature and density calculated in this way and used for the atomic-physics simulations. According to the plot of Fig. 8, the electron temperature increases rapidly during the rise time of the pulse and reaches a plateau at approximately 400 eV. The plateau lasts approximately 2 ns, a duration significantly shorter than the FWHM of the laser pulse. In contrast, the plot of Fig. 9 shows that the electron density increases up to 3×10^{21} cm^{-3} at the peak of the laser pulse and decreases as the laser intensity decreases, having a value of approximately 4×10^{20} cm^{-3} 1.5 ns after the peak of the laser pulse.

It is worthwhile noting that an evaluation of the atomic relaxation times at the densities and temperatures reached during the rise time of the laser pulse (namely, at about 1 ns before its peak) indicates that transient ionization effects are expected to occur. A discussion of this issue has been already given in Ref. 29, where the prediction for the history of the Lyα-to-Heβ intensity ratio was shown, obtained by postprocessing the histories of temperature and density shown in Figs. 8 and 9 with the code FLY in both SS and TD conditions. A comparison with the experimental results showed a good agreement only for the TD simulation. Here we point out the role played by our interaction geometry in the rapid

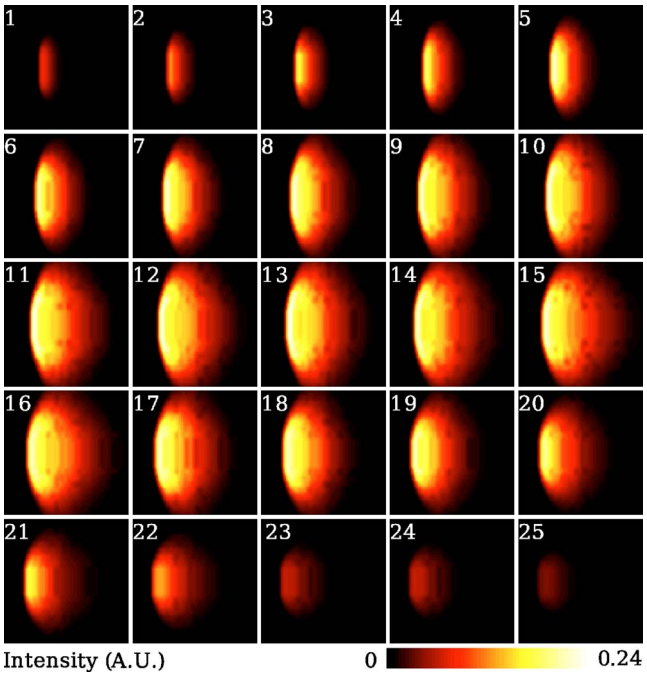

FIG. 6. (Color online). Calculated 2D maps of the x-ray emission at the Heβ line at different times with respect to the peak of the laser pulse. Each frame corresponds to a different time with respect to the peak of the laser pulse, located at frame No. 13. The time interval between successive frames is 100 ps, so that frame No. 1 (No. 25) corresponds to 1.2 ns before (after) the pulse peak. The horizontal scale goes from −25 to 75 μm, the original target surface being located at 0 μm and the laser beam impinging from the right. The vertical scale ranges from −25 to 25 μm. The intensity is normalized to the maximum of the Lyα and the Heβ emissivity during the whole pulse duration.

evolution in the hydrodynamic conditions. In contrast, the effect of the x-ray reabsorption have not been discussed in that Letter and will be carefully concerned in what follows.

C. Opacity effects

As discussed above, opacity issues are of a crucial importance when modeling x-ray spectra from laser plasmas. We used the kinetic code FLY to take into account reabsorption in a homogeneous plasma slab through the escape factors. The slab thickness was taken from the longitudinal profile of the ground-state populations of the He-like and H-like

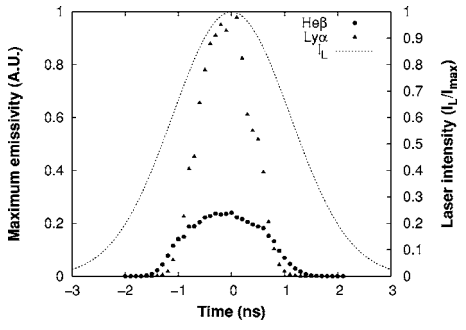

FIG. 7. Calculated maximum local values, as taken from each frame of the maps of Figs. 5 and 6, of the emissivity for the Lyα and Heβ lines as a function of time. The relative intensity I_L/I_{max} of the incident laser pulse is also shown.

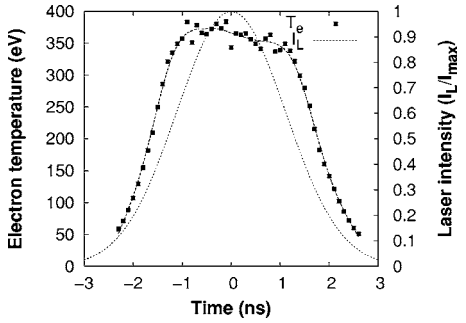

FIG. 8. Calculated history of the electron temperature of the region where the emission of the Heβ line is maximum. The relative intensity I_L/I_{max} of the incident laser pulse is also shown.

ions as retrieved by postprocessing POLLUX simulations using FLY. Figure 10 shows the Lyα-to-Heβ intensity ratio as simulated by FLY, in time-dependent conditions, using a plasma slab thickness equal to the width of the profile of the He-like ground-state population taken at 10%, 50%, and 90% of its maximum. In addition, the curve obtained assuming a zero-width plasma slab (no opacity) is also shown. These curves are compared with the experimental Lyα-to-Heβ ratio, also shown in the figure. The comparison shows that an agreement is found only when the width of the slab to be used in the simulation is the smallest possible. The same conclusion can be obtained when the profiles of the H-like ion population are considered. In other words, we can conclude that, in spite of the relatively large plasma extension, both the Lyα and Heβ lines are optically thin in our conditions. As we will see below, the Doppler decoupling mechanism[40] in the expanding plasma may provide a reasonable explanation to this experimental observation.

D. Effect of the velocity gradient

As shown in Ref. 18, when the effect of the velocity gradient is taken into account in radiative-transfer calculations, strong asymmetries can appear in the line shapes. This is due to the different reabsorption probabilities for the photons at slightly different frequencies due to the Doppler effect.[40] This is a very important issue when attempting to model x-ray spectra from laser plasmas. On the other hand, this effect can lead to a simplification of the radiative-transfer problem when strong gradients exist in the

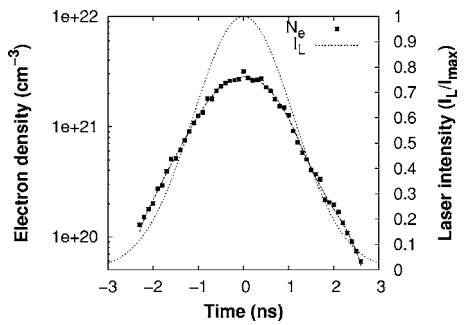

FIG. 9. Calculated history of the electron density of the region where the emission of the Heβ line is maximum. The relative intensity I_L/I_{max} of the incident laser pulse is also shown.

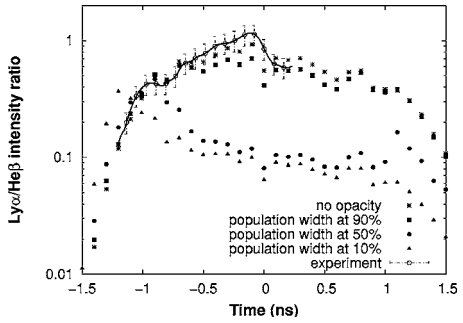

FIG. 10. Lyα-to-Heβ intensity ratio as calculated by the code FLY in time-dependent conditions using a plasma slab whose size as a function of time is taken from the width of the longitudinal profile of the He-like ion ground-state population. The experimental values of the ratio obtained from time-resolved x-ray spectroscopy are also shown.

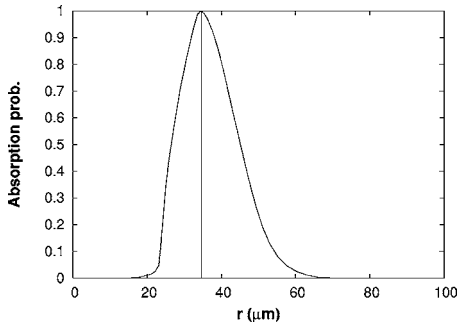

FIG. 12. Probability of a photon at the Lyα wavelength to be reabsorbed in the plasma as calculated using formula (2). r is the coordinate along the line of sight of the plasma and passing through the longitudinal position (marked by the vertical line) where, according to Fig. 5, the emission at the Lyα wavelength exhibits a maximum.

plasma.[41,42] This so-called Doppler decoupling mechanism is likely to occur in our experiment due to the tight-focusing condition and the resulting spherical expansion geometry. In order to estimate the role of this mechanism on our measurements we consider the profile of the component along the line of sight of the fluid velocity of the plasma as provided by the code POLLUX. Figure 11 shows, in particular, this profile for the line passing through the point at which the maximum of the Lyα line emission occurs (at the time of the maximum laser intensity). This profile shows the presence of a strong velocity gradient (of about 5×10^9 s^{-1}) near this point (a similar result holds for the Heβ line emission). This holds, in particular, during the rising of the laser pulse and up to its maximum.

A quantitative evaluation of the Doppler decoupling mechanism in our case can be obtained by estimating the probability for a photon emitted by an element of plasma at a position r_1, temperature T_1, and velocity v_1, to be reabsorbed in r_2, where the corresponding values are T_2 and v_2 (r is a coordinate along the line of sight). In principle, this probability depends upon the superposition integral of the line shapes at the two points and upon the density of the ions in the lower level involved in the transition. Also we consider that, due to the rapid spatial changes in the ion density for each charge state, the maximum of the emissivity for each atomic state actually occurs where the corresponding ion population is maximum. In these circumstances, we can retrieve an upper limit to this probability by considering only the superposition integral

$$I(r_1,r_2)\propto\int d\omega\exp\left[-\frac{(\omega-\omega_1)^2}{2\sigma_1^2}\right]\exp\left[-\frac{(\omega-\omega_2)^2}{2\sigma_2^2}\right].$$

Here ω_1 and ω_2 are the central frequencies of the line as seen in the laboratory frame, that is,

$$\omega_{1,2}=\omega_0\left(1+\frac{v_{1,2}}{c}\right),$$

ω_0 being the line frequency in the ion's rest frame. Furthermore, the linewidths depend on the (ion) temperature at each point:

$$\sigma_{1,2}=\sigma_{1,2}(T_{1,2}).$$

The above argument is valid provided that, as in our case, the coordinate r_1 (for each of the Lyα and the Heβ line) corresponds to where, according to the longitudinal profiles of Figs. 5 and 6, the maximum of the emission occurs. In other words, the following quantity was calculated:

$$P(r)=\frac{I(r_{\max},r)}{I(r_{\max},r_{\max})}. \tag{2}$$

Figure 12 shows the result of this calculation for the Lyα line, using the profile for the fluid velocity and the electron temperature retrieved by the hydrodynamic modeling. As it was said above, r is a coordinate along the line of sight of the plasma passing through the longitudinal position where the emission at the Lyα wavelength has a maximum. According to this plot, the reabsorption probability for a Lyα wavelength photon drops to 50% just a few microns away from the location where the photon is emitted (a very similar result holds for a Heβ photon). In other words, the portion of plasma where reabsorption can occur efficiently is typically smaller than the width of the emitting slab. This simple analytical estimate confirms that Doppler decoupling may play an important role in the radiation transport in our point-like plasma. Further experimental work could be done to study the plasma opacity in our point-like plasma as a function of the line of sight. However, the above argument suggests that

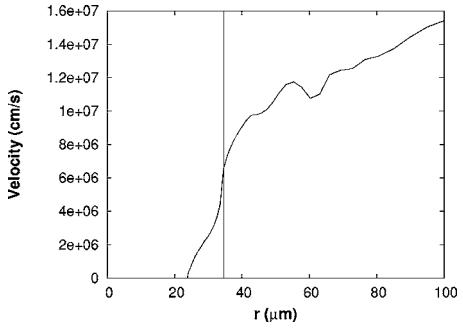

FIG. 11. Profile of the component along the line of sight of the fluid velocity of the plasma as provided by the code POLLUX at the peak of the laser pulse. The vertical line marks the point at which the maximum of the Lyα line emission occurs.

Doppler decoupling may account for a sizable reduction of opacity effects in this experimental configuration.

IV. SUMMARY AND CONCLUSIONS

In this paper the study of a point-like ns laser-produced Al plasma, that is, of a plasma produced by tight-focusing irradiation of a solid Al target, has been reported. The hydrodynamic and atomic-physics features of such a plasma have been studied by comparing experimental x-ray-emission data with predictions by a 2D hydrodynamic and a collisional-radiative kinetic code. In particular, hydrodynamic simulations show that the expansion of the plasma exhibits strong longitudinal gradients of the electron density and temperatures as well as of the fluid velocity. 2D emission maps for the Lyα and Heβ lines were obtained by postprocessing the hydrodynamic data with a time-dependent atomic-physics code. These maps clearly show that, due to the rapid expansion cooling, x-ray emission originates predominantly from a well-localized plasma region characterized by rapidly evolving hydrodynamic conditions. Furthermore, this last issue yields a measurable discrepancy between the experimental line intensity ratios and the ones simulated using a steady-state approximation.

A study of the effect of the large velocity gradients on the line reabsorption in this experimental condition has also been performed, which shows that Doppler decoupling may have an important role, possibly leading to a reduction of the line opacity.

These results show that the experimental configuration described in this work can be profitably used to investigate general issues concerning the atomic and hydrodynamic features of a ns laser plasma.

[1] M. Segers, M. Bougeard, E. Caprin *et al.*, Microelectron. Eng. **61–62**, 139 (2002).
[2] D. Batani, C. Botto, M. Moret *et al.*, Eur. Phys. J. D **21**, 167 (2002).
[3] E. Andersson, G. Hölzer, E. Förster, M. Gratz, L. Kieman, A. Sjögren, and S. Svanberg, Appl. Phys. (N.Y.) **90**, 3048 (2001).
[4] J. C. Kieffer, A. Krol, Z. Jiang, C. C. Chamberlain, E. Scalzetti, and Z. Ichalalene, Appl. Phys. B: Lasers Opt. **74**, S75 (2002).
[5] J. Dunn, A. L. Osterheld, R. Shepherd, W. E. White, V. N. Shlyaptsev, and R. E. Stewart, Phys. Rev. Lett. **80**, 2825 (1998).
[6] C. Deutsch, Eur. Phys. J.: Appl. Phys. **24**, 95 (2003).
[7] S. E. Bodner, D. G. Colombant, J. H. Gardner *et al.*, Phys. Plasmas **5**, 1901 (1998).
[8] D. D. Ryutov, B. A. Remington, H. F. Robey, and R. P. Drake, Phys. Plasmas **8**, 1804 (2001).
[9] L. A. Gizzi, A. Giulietti, D. Giulietti *et al.*, Phys. Rev. E **49**, 5628 (1994).
[10] M. Borghesi, A. Giulietti, D. Giulietti, L. A. Gizzi, A. Macchi, and O. Willi, Phys. Rev. E **54**, 6769 (1996).
[11] D. Giulietti, M. Galimberti, A. Giulietti, L. A. Gizzi, P. Tomassini, M. Borghesi, V. Malka, S. Fritzler, M. Pittman, and K. Taphouc, Phys. Plasmas **9**, 3655 (2002).
[12] P. Squillacioti, M. Galimberti, L. Labate, P. Tomassini, A. Giulietti, V. Shibkov, and F. Zamponi, Phys. Plasmas **11**, 226 (2004).
[13] D. M. Chambers, P. A. Pinto, J. Hawreliak *et al.*, Phys. Rev. E **66**, 026410 (2002).
[14] S. H. Glenzer, K. G. Estabrook, R. W. Lee, B. J. Mac-Gowan, and W. Rozmus, J. Quant. Spectrosc. Radiat. Transf. **65**, 253 (2000).
[15] M. E. Foord, S. H. Glenzer, R. S. Thoe, K. L. Wong, K. B. Fornier, B. G. Wilson, and P. T. Springer, Phys. Rev. Lett. **85**, 992 (2000).
[16] R. F. Smith, J. Dunn, J. Nielsen *et al.*, Phys. Rev. Lett. **89**, 065004 (2002).
[17] H. R. Griem, *Principles of Plasma Spectroscopy* (Cambridge University Press, Cambridge, 1997).
[18] P. K. Patel, J. S. Wark, D. J. Heading, A. Djaoui, S. J. Rose, O. Renner, and A. Hauer, J. Quant. Spectrosc. Radiat. Transf. **57**, 683 (1997).
[19] J. P. Christiansen, D. E. T. F. Ashby, and K. V. Roberts, Comput. Phys. Commun. **7**, 271 (1974).
[20] A. Djaoui and S. J. Rose, J. Phys. B **25**, 2745 (1992).
[21] D. Riley, J. Quant. Spectrosc. Radiat. Transf. **60**, 221 (1998).
[22] P. Sondhauss, S. J. Rose, R. W. Lee, I. Al'miev, and J. S. Wark, J. Quant. Spectrosc. Radiat. Transf. **71**, 721 (2001).
[23] R. W. Lee, J. K. Nash, and Y. Ralchenko, J. Quant. Spectrosc. Radiat. Transf. **58**, 737 (1997).
[24] L. Aschkem, S. Depierreux, K. G. Estabrook *et al.*, J. Quant. Spectrosc. Radiat. Transf. **65**, 23 (2000).
[25] L. A. Gizzi, A. Giulietti, O. Willi, and D. Riley, Phys. Rev. E **62**, 2721 (2000).
[26] O. Renner, J. Limpouch, E. Krousky, I. Uschmann, and E. Förster, J. Quant. Spectrosc. Radiat. Transf. **81**, 385 (2003).
[27] D. M. Chambers, S. H. Glenzer, J. Hawreliak *et al.*, J. Quant. Spectrosc. Radiat. Transf. **71**, 237 (2001).
[28] M. Fajardo, P. Audebert, P. Renaudin, H. Yashiro, R. Shepherd, J. C. Gauthier, and C. Chenais-Popovics, Phys. Rev. Lett. **86**, 1231 (2001).
[29] L. A. Gizzi, C. A. Cecchetti, M. Galimberti, A. Giulietti, D. Giulietti, L. Labate, S. Laville, and P. Tomassini, Phys. Plasmas **10**, 4601 (2003).
[30] L. A. Gizzi, Ph.D. thesis, University of London, 1994.
[31] L. Labate, M. Galimberti, A. Giulietti, D. Giulietti, L. A. Gizzi, and R. Numico, Laser Part. Beams **20**, 223 (2002).
[32] A. A. Hauer, N. D. Delamater, and Z. M. Koenig, Laser Part. Beams **9**, 3 (1991).
[33] L. Labate, Ph.D. thesis, Università di Bologna, Italy, 2004.
[34] G. J. Pert, J. Comput. Phys. **43**, 111 (1981).
[35] G. J. Pert, J. Plasma Phys. **41**, 263 (1989).
[36] C. E. Max, in *Laser-Plasma Interaction*, Proceedings of the Les Houches Summer School, session XXXIV, edited by R. Balian and J. C. Adam (North-Holland, Amsterdam, 1982).
[37] R. W. Lee and J. T. Larsen, J. Quant. Spectrosc. Radiat. Transf. **56**, 535 (1996).
[38] S. J. Pestehe and G. J. Tallents, J. Quant. Spectrosc. Radiat. Transf. **72**, 853 (2002).
[39] L. Labate, M. Galimberti, A. Giulietti, D. Giulietti, L. A. Gizzi, R. Numico, and A. Salvetti, Laser Part. Beams **19**, 117 (2001).
[40] W. Brunner and R. W. John, Laser Part. Beams **9**, 817 (1991).
[41] P. K. Patel, E. Wolfrum, O. Renner, A. Loveridge, R. Allott, D. Neely, S. J. Rose, and J. S. Wark, J. Quant. Spectrosc. Radiat. Transf. **65**, 429 (2000).
[42] J. S. Wark, A. Djaoui, S. J. Rose, H. He, O. Renner, T. Missalla, and E. Förster, Phys. Rev. Lett. **72**, 1826 (1994).